Journal of Biomechanics 79 (2018) 232–237

Contents lists available at ScienceDirect

Journal of Biomechanics

journal homepage: www.elsevier.com/locate/jbiomech
www.JBiomech.com

Short communication

Flow rates in perfusion bioreactors to maximise mineralisation in bone tissue engineering *in vitro*

Feihu Zhao [a,b], Bert van Rietbergen [a], Keita Ito [a,b,c], Sandra Hofmann [a,b,*]

[a] Orthopaedic Biomechanics Group, Department of Biomedical Engineering, Eindhoven University of Technology, PO Box 513, 5600 MB Eindhoven, The Netherlands
[b] Institute for Complex Molecular Systems (ICMS), Eindhoven University of Technology, PO Box 513, 5600 MB Eindhoven, The Netherlands
[c] Department of Orthopaedics, UMC Utrecht, PO Box 85500, 3508 GA Utrecht, The Netherlands

ARTICLE INFO

Article history:
Accepted 10 August 2018

Keywords:
Computational fluid dynamics
wall shear stress
mechanical stimulation
bone tissue mineralisation

ABSTRACT

In bone tissue engineering experiments, fluid-induced shear stress is able to stimulate cells to produce mineralised extracellular matrix (ECM). The application of shear stress on seeded cells can for example be achieved through bioreactors that perfuse medium through porous scaffolds. The generated mechanical environment (i.e. wall shear stress: WSS) within the scaffolds is complex due to the complexity of scaffold geometry. This complexity has so far prevented setting an optimal loading (i.e. flow rate) of the bioreactor to achieve an optimal distribution of WSS for stimulating cells to produce mineralised ECM. In this study, we demonstrate an approach combining computational fluid dynamics (CFD) and mechano-regulation theory to optimise flow rates of a perfusion bioreactor and various scaffold geometries (i.e. pore shape, porosity and pore diameter) in order to maximise shear stress induced mineralisation. The optimal flow rates, under which the highest fraction of scaffold surface area is subjected to a wall shear stress that induces mineralisation, are mainly dependent on the scaffold geometries. Nevertheless, the variation range of such optimal flow rates are within 0.5–5 mL/min (or in terms of fluid velocity: 0.166–1.66 mm/s), among different scaffolds. This approach can facilitate the determination of scaffold-dependent flow rates for bone tissue engineering experiments *in vitro*, avoiding performing a series of trial and error experiments.

1. Introduction

In bone tissue engineering (BTE) experiments *in vitro*, cells grown on porous 3D scaffolds in osteoinductive media can be stimulated to mineralise their extracellular matrix (ECM). This can be further enhanced by mechanical stimulation of the cells (i.e. fluid-induced shear stress) (Bancroft et al., 2002; Gomes et al., 2006; Li et al., 2009; Sikavitsas et al., 2003; Vetsch et al., 2017). For instance, ECM could be mineralised within silk fibroin (SF) scaffolds when cells were subjected to a wall shear stress (WSS) between 1.47 mPa and 24 mPa (Vetsch et al., 2017). In another study by Li et al. (2009), mineralised bone-like tissue would be formed within the β-tricalcium phosphate (β-TCP) scaffolds (porosity = 75% and pore diameter = 530 ± 100 μm) when cells were subjected to a WSS of 5–15 mPa. When bone marrow stromal cells were cultured within a titanium fiber mesh (porosity = 86%), the WSS ranges for inducing mineralisation were between 10 and 30 mPa (Sikavitsas et al., 2003). While an excessively high WSS (i.e. over 60 mPa) was shown to result in cell death/detachment (McCoy et al., 2012; Olivares et al., 2009), a rather low WSS (i.e. <0.11 mPa) could not stimulate the cells to produce mineralised ECM (Olivares et al., 2009). In BTE experiments where cells are attached to scaffold walls/surfaces, it would be desirable that the WSS can be controlled within the range for inducing mineralisation of the ECM. One way to do so is through the use of perfusion bioreactors. One of the challenges with such a system is to determine the external flow rate, controlled by the experimenter, for which most of the scaffold surface is exposed to a WSS in the range for inducing ECM mineralisation. Often, the selection of the external flow rate is based on trial-and-error studies, and only valid for the specific experimental setup. Since the applied flow rate that induces mineralisation would depend on fluid-flow characteristics, bioreactor design and the scaffold, flow rates between different groups are hard to compare. Consequently, a wide range of applied flow rates has been reported (Bancroft et al., 2002; Grayson et al., 2008; Porter et al., 2007; Vetsch et al., 2017; Yeatts and Fisher, 2011). To date, no systematic approach has been proposed to

* Corresponding author at: Orthopaedic Biomechanics Group, Department of Biomedical Engineering, Eindhoven University of Technology, PO Box 513, 5600 MB Eindhoven, The Netherlands.
E-mail address: S.Hofmann.Boss@tue.nl (S. Hofmann).

https://doi.org/10.1016/j.jbiomech.2018.08.004
0021-9290/

calculate the fluid flow in such a way that it can lead to maximising the mineralising ECM in more areas within scaffolds. Given the large number of parameters involved (i.e. the fluid-flow characteristics, the bioreactor- and scaffold design), optimisation of the applied flow rate in a trial-and-error fashion is not time- and cost-effective and cannot easily be translated to other designs (Geris et al., 2016).

In this study, we aim to calculate the optimal fluid flow rate to be applied to the bioreactor for BTE experiments. The optimal flow rate calculation was based on the objective to maximise the scaffold surface fraction, which is subjected to a WSS in a range for stimulating mineralisation as reported by previous mechanoregulation theories. Using a computational fluid dynamics (CFD) approach, the actual WSS at the scaffold surface was calculated for different scaffold pore shapes, pore diameters and porosities as a function of the applied fluid flow rates. For each case the optimal flow rate was determined. It is anticipated that this calculated optimal loading approach could facilitate BTE experimentalists to determine the applied loading (i.e. flow rate) for achieving a higher amount of mineralised bone tissue, when a perfusion bioreactor is used in experiments.

2. Methods

A computational fluid dynamics (CFD) model was developed for a perfusion bioreactor (Fig. 1) to compute the WSS distribution within scaffolds. As the bioreactor was axially symmetric, and the scaffold was homogeneous, only one quarter of the bioreactor was modelled (Fig. 1). According to a pre-computation using a commercial CFD package, CFX (ANSYS Inc. USA), the maximal Reynold number was 39.5, which was within the laminar flow range. Thus, the fluid flow was defined as a laminar Newtonian flow with the WSS on the scaffold surface (Γ_S) being calculated as in Eq. (1) (Tanaka et al., 2012):

$$\tau_{ij} = \mu\left(\frac{\partial v_i}{\partial x_j} + \frac{\partial v_j}{\partial x_i}\right)\Big|_{x_i \in \Gamma_s} \quad (1)$$

where μ is the dynamic viscosity of cell culture medium (Dulbecco's Modified Eagle medium supplemented with 10% FBS) with a value of 1.0 mPa s (Maisonneuve et al., 2013); v_i (or v_j) is the velocity vector in direction of i (or j); x_i (or x_j) is the ith (or jth) spatial coordinates.

On the two cutting surfaces, the fluid velocity followed Eq. (2):

$$\begin{cases} v_j = 0 \\ \frac{\partial v_i}{\partial x_j} = 0 \end{cases} \quad (2)$$

with j being the direction perpendicular to the cutting surface.

The bioreactor walls and the scaffold surfaces were defined as non-slip, on which the fluid had zero velocity (Fig. 1). According to the applied loading in previous experiments (Bancroft et al., 2002; Gomes et al., 2003; Li et al., 2009; Vetsch et al., 2017), different flow rates (0.1–12 mL/min) were applied to the inlet, while the relative pressure at the outlet was defined as zero. The WSS at the scaffold surface was calculated for these different fluid-flow rates. From this, the surface area fraction that was stimulated to mineralise was calculated, according to a mechano-regulation theory whereby ECM mineralisation would be stimulated when WSS was in a certain range, i.e. τ = 1.47–24 mPa (Vetsch et al., 2017), τ = 5–15 mPa (Li et al., 2009), τ = 10–30 mPa (Sikavitsas et al., 2003). For each of the described external flow rates, the surface area fraction, whose WSS was in the range specified by these criteria was calculated, and the value that resulted in the highest surface fraction was selected as the optimal flow rate as described in Appendix A.

Supplementary data associated with this article can be found, in the online version, at https://doi.org/10.1016/j.jbiomech.2018.08.004.

To investigate the influence of scaffold geometry on the applied flow rates, the scaffold pore shape, pore diameter and porosity were varied as described in Table 1. The reason of selecting these scaffolds and scaffold geometric analysis were presented in Appendix B. A local curvature-dependent mesh strategy was employed for meshing the fluid domain. Specifically, the mesh was subdivided in curved regions until the individual elements span the angle between two neighbouring elements of 75–24° (minimum element edge length = 13 μm). The mesh on the interface between scaffold and fluid was refined with a maximum element size of 60 μm after mesh sensitivity analysis. Finally, the ANSYS CFX solver resolved the models using a finite volume method under the convergence criteria of root-mean-square residual of the mass and momentum $<1 \times 10^{-4}$.

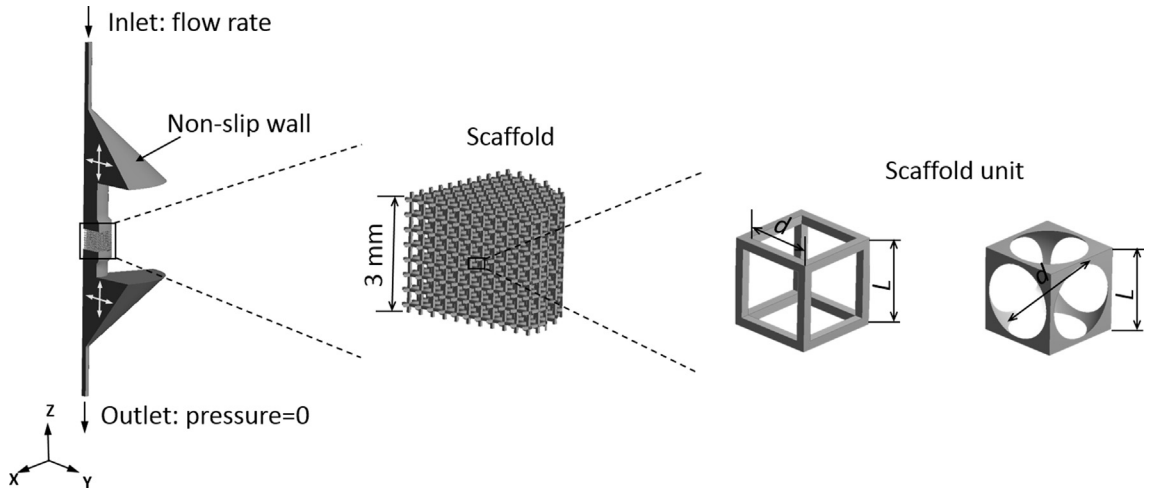

Fig. 1. One quarter of the fluid domain in the bioreactor for the CFD analysis. The scaffold in the bioreactor is assembled by repeating units, which have either rectangular or spherical pore shapes. Variable L is the length of the scaffold unit, d is the pore diameter of the scaffold.

Table 1
Variation in scaffold geometry, including (i) the variation of pore shape while porosity and pore diameter are kept constant; (ii) the variation of pore diameter while porosity and rectangular pore shape are kept constant; (iii) the variation of porosity while pore diameter and rectangular pore shape are kept constant.

Pore shape variation	φ = 90%, d = 300 μm		
	Spherical pore	Rectangular pore	
Pore diameter (d) variation	Rectangular pore, φ = 90%		
	d = 200 μm	d = 300 μm	d = 500 μm
Porosity (φ) variation	Rectangular pore, d = 300 μm		
	φ = 50%	φ = 70%	φ = 90%

3. Results

To investigate the effect of the pore shape (rectangular or spherical) on the expected mineralisation, the scaffolds' surface fraction, whose WSS was within the range for ECM mineralisation was calculated according to the different mechano-regulation theories. This investigation was based on a fixed pore size (d = 300 μm) and porosity (φ = 90%) but with varying pore shapes (Fig. 2). For the scaffolds with spherical pores, the flow rates that resulted in the highest surface fraction for mineralisation were in the range of 1–2 mL/min (Fig. 2). For the scaffolds with rectangular pores, optimal flow rates were in the range of 2–3 mL/min.

To investigate the effect of the scaffold pore diameter on the expected mineralisation, the scaffolds' surface fraction, which had the WSS within the range for ECM mineralisation was calculated according to different mechano-regulation theories. These scaffolds had a fixed pore shape (rectangular) and porosity (φ = 90%) but with varying pore diameters (Fig. 3). For the scaffolds with 500 μm pores, the flow rates that resulted in the highest surface fraction for mineralisation were in the range of 3–5 mL/min. For the scaffolds with smaller pore diameters (d = 300 μm and 200 μm), the optimal flow rate was in the range of 2–3 mL/min.

To investigate the influence of the scaffold porosity on the expected mineralisation, similar calculation approach was employed as above. These scaffolds had a fixed pore shape (rectangular) and pore diameter (d = 300 μm) but with varying porosities (Fig. 4). For the scaffolds with the highest porosity (φ = 90%), the flow rates that resulted in the highest surface fraction for mineralisation were in the range of 2–3 mL/min. For the scaffolds with medium (φ = 70%) and low porosity (φ = 50%), such optimal flow rate ranges were shifted to 1–5 mL/min and 0.5–1 mL/min, respectively.

4. Discussion and conclusion

In this study, we employed a combination of CFD with mechano-regulation theories to optimise the external flow rate for a perfusion bioreactor. Such flow rate would maximise the scaffold surface fraction, whose WSS was in the range required for mineralisation. As expected, the optimal flow rate was dependent on the scaffold geometry, in particular on the scaffold porosity. However, it was in a reasonable range of 0.5–5 mL/min for the bioreactor used in our study. To enable a direct translation of our findings to bioreactors with other internal geometries, the optimal flow rate range (0.5–5.0 mL/min) was converted to represent an optimal fluid velocity (0.166–1.66 mm/s). This fluid velocity could be applied to the channel, where the scaffolds are placed.

In an earlier study by Vetsch et al. (2017), the same bioreactor design was used as in this study in combination with silk fibroin scaffolds with a porosity of 90% for BTE experiments. Vetsch et al. (2017) applied both low and high level of flow rates (0.1 mL/min and 12 mL/min) and found no mineralisation under the low flow rate and only small amounts of mineralised tissue under 12 mL/min. Based on our results, we would have predicted that the low fluid flow was too low for inducing mineralisation, while the high rate was too high for cells to survive. Our model would predict optimal mineralisation to occur for a flow rate in the range of 0.5–5 mL/min (0.166–1.66 mm/s). In another study (Li et al., 2009), three flow rates (3 mL/min, 6 mL/min and 9 mL/min) were applied to a perfusion bioreactor, and the highest mineralisation within the scaffold (porosity = 75% and pore diameter = 530 ± 100 μm) was found under the flow rate of 3 mL/min (0.32 mm/s). This corresponds well with our findings, although their results were obtained in a bioreactor with a different geometry.

One of the limitations in this study was the assumption that cells were attached uniformly on the scaffold surface. However, it could also be possible for the cells to bridge across the pores, which might induce different loads on the cells. It has been shown that the maximum WSS on cells bridging over pores can be lower than WSS on cells attached flat on the scaffold surface, if the cells do not

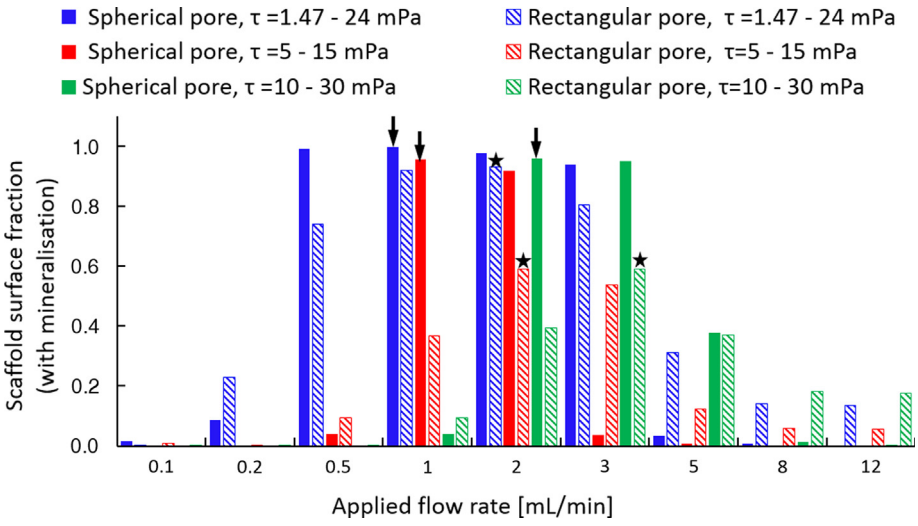

Fig. 2. Influence of the applied flow rate on the mineralised scaffold surface: the scaffolds have different pore shapes (i.e. spherical and rectangular shapes) with a constant pore diameter of 300 μm and porosity of 90%. The highest scaffold surface area fractions with mineralisation based on different τ for inducing mineralisation are pointed out by arrow (for spherical pore shape) and star (for rectangular pore shape).

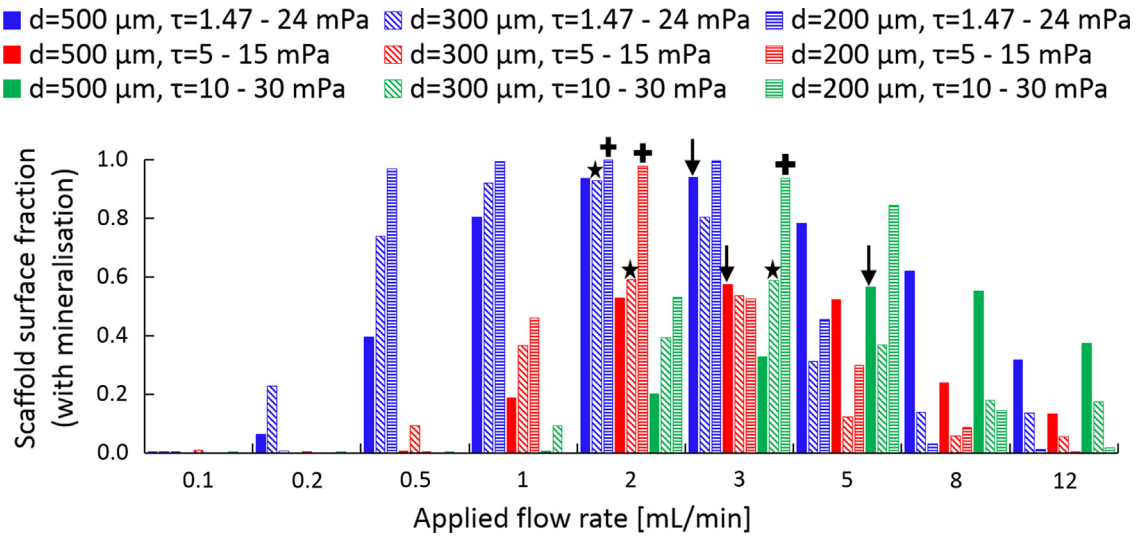

Fig. 3. Influence of the applied flow rate on the mineralised scaffold surface: the scaffolds have different pore diameters d (i.e. d = 200–500 μm) with a constant porosity of 90% and rectangular pore shape. The highest scaffold surface area fractions with mineralisation based on different τ for inducing mineralisation are pointed out by arrow (for d = 500 μm), star (for d = 300 μm) and cross (for d = 200 μm).

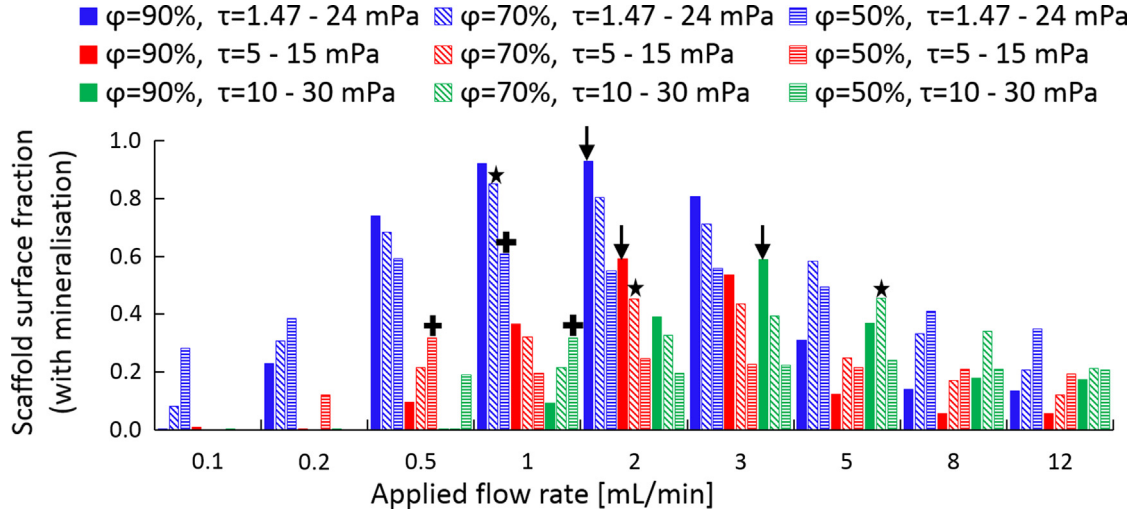

Fig. 4. Influence of the applied flow rate on the mineralised scaffold surface: the scaffolds have different porosities φ (i.e. φ = 50–90%) with a constant pore size of 300 μm and rectangular pore shape. The highest scaffold surface area fractions with mineralisation based on different τ for inducing mineralisation are pointed out by arrow (for φ = 90%), star (for φ = 70%) and cross (for φ = 50%).

face the mainstream of the flow within scaffold pores (Guyot et al., 2016b). This was in line with the findings in another study (Zhao et al., 2015). In addition, it was also found previously by Zhao et al. (2015) that if cells attaching to the scaffold surface and cells bridging over pores both faced the mainstream of the medium flow within the scaffold pores, a higher WSS would impart on bridged cells. Another limitation was the use of scaffolds with an idealised homogeneous geometry for precisely controlling the geometrical features (i.e. pore shape, porosity and pore diameter). However, in reality, the scaffold could have a non-uniform pore size distribution or porosity due to the variability in the manufacturing process for example. This might result in a different WSS distribution within the whole scaffold. For example, Melchels et al. (2011) simulated the fluidic environment within a polymerisable poly(D,L-lactide) (PDLLA) scaffold with non-uniform porosities (40–85%). It was found that the wall shear rate was varying between 15 s^{-1} and 40 s^{-1} within the whole scaffold (Melchels et al., 2011). This implied that in a scaffold with a less regular or less uniform pore geometry, a larger variation in WSS could be seen. If the WSS variation was not large, and sat within the WSS range for mineralisation, the amount of cells that received the WSS for mineralisation would not change. If the WSS variation was larger than the WSS range for mineralisation, fewer cells would be stimulated to produce mineralised ECM under optimal loading conditions. In addition, our study was based on mechano-regulated mineralisation only, while nutrient delivery could also affect tissue growth (Mehrian et al., 2018; Nava et al., 2013; Zhao et al., 2017). This will particularly play a role at low flow rates (i.e. = 0.5 mL/min) and needs to be taken into account when operating these. Finally, our results are only valid for the initial stage of the mineralisation process. Once tissue is being deposited by the cells, the fluid flow through the scaffold would change. This would change the WSS and its distribution (Guyot et al., 2015; Guyot et al., 2016a; Nava et al., 2013). Meanwhile, such changes of WSS would affect the

Table 2
Recommended fluid velocities ranges that can be applied by flow perfusion bioreactors to maximise ECM mineralisation.

		Applied fluid velocity [mm/s]								
		0.03	0.07	0.17	0.33	0.66	1.00	1.66	2.66	3.98
Variation of pore shapes	Spherical				■	■				
	Rectangular					■	■			
Variation of pore diameters (d)	d = 200 μm					■	■			
	d = 300 μm					■	■			
	d = 500 μm						■	■		
Variation of porosities (φ)	φ = 50%			■	■					
	φ = 70%				■	■	■	■		
	φ = 90%					■	■			

ECM formation due to the coupling nature of WSS and ECM formation (Guyot et al., 2015; Guyot et al., 2016a; Nava et al., 2013). It is likely that the amount of mineralised ECM will be influenced by the WSS change due to ECM growth within the scaffold. Therefore, future models for predicting the ECM mineralisation under WSS should take into account tissue formation over time.

The results in this study showed that the most distinct influence on the optimal flow rates was given by the scaffold porosity. However, a previous computational study found that the scaffold pore diameter had the most distinct influence (Zhao et al., 2016). This mismatch could be explained by the different calculation criteria the study used to define the optimal fluid flow. While Zhao et al. (2016) merely focused on the relationship between average WSS and pore diameter, our study optimised the scaffold surface fraction that was in the range required for mineralisation. In our study, it was found that the 'overall optimal' flow rate range for mineralisation was considerably narrower than those applied in previous experiments (i.e. 0.1–12 mL/min). However, the optimal flow rate range still had a 10-fold margin (i.e. 0.5–5.0 mL/min). One reason was that we applied different WSS ranges for stimulating ECM mineralisation to calculate the optimal flow rates. Another reason was the influence of scaffold geometries, which showed a distinct influence on the optimal flow rates. For a particular experimental setup, a specific optimal flow rate can be derived from the information in Figs. 2–4 and Table 2.

In conclusion, with the approach outlined in this study, it is possible to calculate optimal flow rates for BTE experiments. Since the approach is based on a cell level WSS criterion obtained from mechano-biological experiments, it will provide consistent results also when using different scaffolds or bioreactor designs. We thus expect that this approach can lead to the reduction of pilot studies required to find optimal loading conditions as well as to a better insight into the parameters that determine the mineralisation within scaffolds.

Acknowledgement

The authors FZ and SH acknowledge funding from the EU Seventh Framework Programme (FP7/2007-2013); grant agreement number 336043 (project REMOTE). Additionally, we would like to thank Johanna Melke (TU Eindhoven) and Prof. Damien Lacroix (University of Sheffield) for valuable discussions, as well as Dr. Myles Mc Garrigle (NUI Galway) for proof-reading the manuscript.

Conflict of interests

The authors declare that no conflict of interests are involved in this paper.

References

Bancroft, G.N., Sikavitsas, V.I., van den Dolder, J., Sheffield, T.L., Ambrose, C.G., Jansen, J.A., Mikos, A.G., 2002. Fluid flow increases mineralized matrix deposition in 3D perfusion culture of marrow stromal osteoblasts in a dose-dependent manner. PNAS 99, 12600–12605.

Geris, L., Guyot, Y., Schrooten, J., Papantoniou, I., 2016. In silico regenerative medicine: how computational tools allow regulatory and financial challenges to be addressed in a volatile market. Interf. Focus 6, 20150105.

Gomes, M.E., Holtorf, H.L., Reis, R.L., Mikos, A.G., 2006. Influence of the porosity of starch-based fiber mesh scaffolds on the proliferation and osteogenic differentiation of bone marrow stromal cells cultured in a flow perfusion bioreactor. Tissue Eng. 12, 801–809.

Gomes, M.E., Sikavitsas, V.I., Behravesh, E., Reis, R.L., Mikos, A.G., 2003. Effect of flow perfusion on the osteogenic differentiation of bone marrow stromal cells cultured on starch-based three-dimensional scaffolds. J. Biomed. Mater. Res. Part A 67, 87–95.

Grayson, W.L., Bhumiratana, S., Cannizzaro, C., Chao, P.H., Lennon, D.P., Caplan, A.I., Vunjak-Novakovic, G., 2008. Effects of initial seeding density and fluid perfusion rate on formation of tissue-engineered bone. Tissue Eng. Part A 14, 1809–1820.

Guyot, Y., Luyten, F.P., Schrooten, J., Papantoniou, I., Geris, L., 2015. A three-dimensional computational fluid dynamics model of shear stress distribution during neotissue growth in a perfusion bioreactor. Biotechnol. Bioeng.

Guyot, Y., Papantoniou, I., Luyten, F.P., Geris, L., 2016a. Coupling curvature-dependent and shear stress-stimulated neotissue growth in dynamic bioreactor cultures: a 3D computational model of a complete scaffold. Biomech. Model. Mechanobiol. 15, 169–180.

Guyot, Y., Smeets, B., Odenthal, T., Subramani, R., Luyten, F.P., Ramon, H., Papantoniou, I., Geris, L., 2016b. Immersed boundary models for quantifying flow-induced mechanical stimuli on stem cells seeded on 3D scaffolds in perfusion bioreactors. PLoS Comput. Biol. 12, e1005108.

Li, D., Tang, T., Lu, J., Dai, K., 2009. Effects of flow shear stress and mass transport on the construction of a large-scale tissue-engineered bone in a perfusion bioreactor. Tissue Eng. Part A 15, 2773–2783.

Maisonneuve, B.G., Roux, D.C., Thorn, P., Cooper-White, J.J., 2013. Effects of cell density and biomacromolecule addition on the flow behavior of concentrated mesenchymal cell suspensions. Biomacromolecules 14, 4388–4397.

McCoy, R.J., Jungreuthmayer, C., O'Brien, F.J., 2012. Influence of flow rate and scaffold pore size on cell behavior during mechanical stimulation in a flow perfusion bioreactor. Biotechnol. Bioeng. 109, 1583–1594.

Mehrian, M., Guyot, Y., Papantoniou, I., Olofsson, S., Sonnaert, M., Misener, R., Geris, L., 2018. Maximizing neotissue growth kinetics in a perfusion bioreactor: an in silico strategy using model reduction and Bayesian optimization. Biotechnol. Bioeng. 115, 617–629.

Melchels, F.P.W., Tonnarelli, B., Olivares, A.L., Martin, I., Lacroix, D., Feijen, J., Wendt, D.J., Grijpma, D.W., 2011. The influence of the scaffold design on the distribution of adhering cells after perfusion cell seeding. Biomaterials 32, 2878–2884.

Nava, M.M., Raimondi, M.T., Pietrabissa, R., 2013. A multiphysics 3D model of tissue growth under interstitial perfusion in a tissue-engineering bioreactor. Biomech. Model. Mechanobiol. 12, 1169–1179.

Olivares, A.L., Marsal, E., Planell, J.A., Lacroix, D., 2009. Finite element study of scaffold architecture design and culture conditions for tissue engineering. Biomaterials 30, 6142–6149.

Porter, B.D., Lin, A.S., Peister, A., Hutmacher, D., Guldberg, R.E., 2007. Noninvasive image analysis of 3D construct mineralization in a perfusion bioreactor. Biomaterials 28, 2525–2533.

Sikavitsas, V.I., Bancroft, G.N., Holtorf, H.L., Jansen, J.A., Mikos, A.G., 2003. Mineralized matrix deposition by marrow stromal osteoblasts in 3D perfusion culture increases with increasing fluid shear forces. PNAS 100, 14683–14688.

Tanaka, M., Wada, S., Nakamura, M., 2012. Computational Biomechanics – Theoretical Background and Biological/Biomedical Problems. Springer Tokyo Dordrecht Heidelberg London New York, Tokyo, Japan.

Vetsch, J.R., Betts, D.C., Müller, R., Hofmann, S., 2017. Flow velocity-driven differentiation of human mesenchymal stromal cells in silk fibroin scaffolds: a combined experimental and computational approach. PLoS One 12, e0180781.
Yeatts, A.B., Fisher, J.P., 2011. Tubular perfusion system for the long-term dynamic culture of human mesenchymal stem cells. Tissue Eng. Part C, Methods 17, 337–348.
Zhao, F., Vaughan, T.J., Mc Garrigle, M.J., McNamara, L.M., 2017. A coupled diffusion-fluid pressure model to predict cell density distribution for cells encapsulated in a porous hydrogel scaffold under mechanical loading. Comput. Biol. Med. 89, 181–189.
Zhao, F., Vaughan, T.J., McNamara, L.M., 2015. Multiscale fluid-structure interaction modelling to determine the mechanical stimulation of bone cells in a tissue engineered scaffold. Biomech. Model. Mechanobiol. 14, 231–243.
Zhao, F., Vaughan, T.J., McNamara, L.M., 2016. Quantification of fluid shear stress in bone tissue engineering scaffolds with spherical and cubical pore architectures. Biomech. Model. Mechanobiol. 15, 561–577.